



HAL
open science

ZSM-5 Monolithic Microreactors with Hierarchical Porosity: Maximizing Selective Production of para-Xylene

Lucie Desmurs, Claudia Cammarano, Alexander Sachse, Olinda Gimello, Thomas Gaillard, Sacha Barberat, Sebastien Blanquer, Vasile Hulea, Anne Galarneau

► **To cite this version:**

Lucie Desmurs, Claudia Cammarano, Alexander Sachse, Olinda Gimello, Thomas Gaillard, et al.. ZSM-5 Monolithic Microreactors with Hierarchical Porosity: Maximizing Selective Production of para-Xylene. Microporous and Mesoporous Materials, 2024, 377, pp.113201. 10.1016/j.micromeso.2024.113201 . hal-04605461

HAL Id: hal-04605461

<https://hal.science/hal-04605461v1>

Submitted on 7 Jun 2024

HAL is a multi-disciplinary open access archive for the deposit and dissemination of scientific research documents, whether they are published or not. The documents may come from teaching and research institutions in France or abroad, or from public or private research centers.

L'archive ouverte pluridisciplinaire **HAL**, est destinée au dépôt et à la diffusion de documents scientifiques de niveau recherche, publiés ou non, émanant des établissements d'enseignement et de recherche français ou étrangers, des laboratoires publics ou privés.

ZSM-5 monolithic microreactors with hierarchical porosity: Maximizing selective production of para-xylene

Lucie Desmurs^a, Claudia Cammarano^a, Alexander Sachse^b, Olinda Gimello^a, Thomas Gaillard^a, Sacha Barberat^a, Sebastien Blanquer^a, Vasile Hulea^a, Anne Galarneau^{a,*}

^a ICGM, Univ Montpellier, CNRS, ENSCM, Montpellier, France

^b IC2MP, Univ Poitiers, CNRS, Poitiers, France

ARTICLE INFO

Keywords:

ZSM-5
MFI
Macroporous
Monolith
Toluene alkylation
para-Xylene
Flow

ABSTRACT

ZSM-5 monoliths with Si/Al ~ 40 were achieved by steam assisted conversion of micro-/macroporous silica-alumina monoliths synthesized by an optimized combination of spinodal decomposition and sol-gel process. ZSM-5 monoliths exhibit a homogeneous and interconnected network of macropores of ~ 30 μm diameter, with a macropore volume of ~ 1 mL g^{-1} and a micropore volume of 0.16 mL g^{-1} , as waited for pure ZSM-5. The skeleton of ZSM-5 monoliths featured a 3D aggregation of spherical particles of 6 μm in diameter. The latter were composed by a stacking of thin plate-like shaped crystallites. The catalytic properties of the ZSM-5 monoliths were assessed through their use as catalytic microreactor in the continuous flow alkylation of toluene with methanol. An outstanding for *para*-xylene selectivity of 81 % was achieved possibly ascribable due to the maximization of pore openings of sinusoidal channels as a result of the plate-like morphology of the ZSM-5 crystallites.

1. Introduction

Zeolites are essential catalysts in the chemical industry [1–3]. Their specific microporous network confers them with unique acidic properties and shape selectivity. By tuning their porous architectures, framework compositions and crystal morphology, catalytic outputs can importantly be affected [3]. An industrially important process is the toluene alkylation with methanol to produce *para*-xylene, a major intermediate used to produce value-added polymers. ZSM-5 zeolites (MFI structure, 10-ring channel system) are the most suitable catalysts for toluene alkylation, which can be explained to their unique pore network [4]. ZSM-5 features two types of interconnected channels: straight channels of circular cross section (0.53×0.56 nm) and sinusoidal channels (also named zigzag channels) of ovoidal cross section (0.51×0.55 nm). The channel intersections give rise to large cavities of ~ 0.8 nm.

Due to the linear shape of *para*-xylene its diffusion is faster in both straight and sinusoidal channels compared to *ortho*- and *meta*-xylene. Yet, isomerization of *para*-xylene into *meta*- and *ortho*-xylene can occur on the external surface of the crystals, often leading to a thermodynamic equilibrium composition of *para*-/*meta*-/*ortho*-xylene of 24 : 52: 24 %

[5]. Hence, maximizing *para*-xylene selectivity in toluene alkylation over ZSM-5 continues to be an important industrial challenge. The main strategies to avoid this secondary isomerization reaction are to minimize the number of acid sites at the external surface of ZSM-5 crystals and/or to increase the diffusion path length for *meta*-xylene and *ortho*-xylene, which can be achieved by maximizing the pore opening through sinusoidal channels [6].

ZSM-5 is usually obtained as nanometer- or micron-sized crystals, which prevents its direct use in flow processes. This explains why in industrial processes zeolites are used as shaped bodies, achieved through the use of binders. These amount of binders used in extrusion processes is typically 30 wt% of the overall composition. The impact of binders, classically clays in extrusion, is far from negligible in catalysis [7–9]. There is hence a tremendous demand to disclose new strategies that allow for shaping pure zeolite bodies, such as monoliths with hierarchical porosity, which further allow for increasing mass transport and easy handling [10]. In order to avoid high column pressure drop monoliths should exhibit macropores superior to 5 μm in diameter [11]. Since 2009 [12] catalysts shaped as monoliths with hierarchical porosity, synthesized by a combination of spinodal decomposition and sol-gel processes [13–16] have allowed for achieving exceptional

outputs in term of selectivity and productivity for continuous catalytic flow processes thanks to their homogeneous macropore network allowing for the perfect control of contact time [10,17–22]. Such catalytic microreactors improve the productivity of catalytic reactions by a factor of 3–10 in comparison to batch reactors and 2 to 3 times in comparison to packed-bed reactors.

The transformation of silica [23–26] or silica-alumina [27,28] based monoliths into pure zeolite monoliths (SOD [23], LTA [24–26], FAU-X [27,28]) was achieved by pseudomorphic transformation, *i.e.* by adjusting the rate of silica dissolution to the rate of zeolites crystallization, allowing for maintaining the shape of the skeleton featuring aggregations of either micro- [23,24] or nanocrystals [25–28] of zeolites. These zeolite monoliths presented outstanding performances when used as catalytic microreactors in Knoevenagel reactions [23,24] and as adsorbents for radioactive metals capture [26,28] in continuous flow.

The pseudomorphic transformation of silica monoliths into beta zeolite was reported by the group of Zhao [29]. The authors modified the silica monoliths with cationic poly (diallyldimethyl)-ammonium chloride (PDDA, 200 kDa) prior to impregnation with a colloidal suspension of beta zeolite seeds. The system was subsequently immersed into a solution of tetraethylammonium hydroxide (TEAOH) and sodium aluminate (NaAlO_2) of composition (Al_2O_3 : $300\text{H}_2\text{O}$: 3 TEAOH). The impregnated seeded monoliths were then subjected to steam assisted conversion (SAC) at 150 °C for 96 h. Resulting beta zeolite monoliths feature a micropore volume of 0.21 mL g^{-1} (corresponding to 87 % of the expected micropore volume of a pure phase), macropores diameter of 2 μm and a skeleton composed of spherical crystals of ca. 0.3–0.4 μm . This beta zeolite monolith was however not tested in catalysis and the acidity was not measured.

The synthesis of ZSM-5 [30] and silicalite-1 [31] monoliths was further reported, achieved through the impregnation of silica monoliths with a solution of aluminum isopropoxide, NaOH and tetrapropylammonium hydroxide (TPAOH) following the molar composition ratio 1 Al_2O_3 : 1 Na_2O : 1266.7 H_2O : 6 TPAOH and subjected to SAC at 150 °C for 24 h [30]. Rather surprisingly the skeleton of the resulting ZSM-5 monolith presented a smooth surface, with the absence of distinguishable crystals. A low micropore volume of 0.09 mL g^{-1} was reported, suggesting a crystallization ratio of 56 %, as the theoretical micropore volume of ZSM-5 is 0.16 mL g^{-1} . NH_3 -TPD analysis gave acidity values of 0.27 mmol H^+ /g. The Si/Al ratio was not reported. Besides the ZSM-5 monolith was not evaluated as catalytic microreactor, but as crushed powder in packed-bed reactor, where it showed higher performance in the cracking of large molecules compared to classical ZSM-5 microporous powder.

To enhance the crystallization degree of the ZSM-5 monoliths, the group of Zhao used another strategy. Here the silica monoliths were first transformed into carbon/silica composites, before their transformation into ZSM-5 [32], silicalite-1 [33] and beta [34] monoliths. The authors achieved full transformation into ZSM-5 monoliths, but again no evaluation as catalytic microreactor was undertaken [32]. A packed-bed column was filled with a crushed fraction of ZSM-5 monoliths, which allowed to achieve similar results in cracking experiments as what was reported by Lei et al. [30]. Yet, a different product selectivity was observed, which suggested a deeper catalytic cracking process, which probably resulting from the presence of large crystals, on which the long diffusion path length allowed for producing secondary cracking products. The Si/Al ratio and the acidity of the ZSM-5 monoliths were not reported.

A further strategy to directly synthesize ZSM-5 monoliths was proposed starting from aluminosilica monoliths (Si/Al = 20), which was impregnated with a TPAOH solution ($1200\text{H}_2\text{O}$: 4 TPAOH) in an ultrasonic bath for 0.5–2 h followed by SAC at 150 °C for 48 h [35]. A high rate of crystallization of ZSM-5 monoliths (micropore volume of 0.15 mL g^{-1}) was reached. The macropores of the resulting ZSM-5 monoliths were small (0.5–1 μm diameter). The Si/Al ratio and the acidity of these ZSM-5 monoliths were not reported. These ZSM-5 monoliths were not

evaluated in catalysis.

Recently, a new approach was proposed by Moukahlal et al. [36] through direct pseudomorphic transformation of silica monoliths into ZSM-5 monoliths using a bifunctional organic surfactant [$\text{C}_{22}\text{H}_{45}\text{-N}^+(\text{CH}_3)_2\text{-C}_6\text{H}_{12}\text{-N}^+(\text{CH}_3)_2\text{-C}_6\text{H}_{13}$]Br₂ at 150 °C for 5 days in a rotating oven followed by a static step at 120 °C for 1 day. The resulting ZSM-5 monoliths featured nanosheet-shaped crystals and a microporous volume of 0.12 mL g^{-1} (corresponding to 75 % of transformation) and presenting very low aluminum incorporation with a final Si/Al ratio of 182.

All ZSM-5 monoliths proposed in the literature featured rather small macropores with diameter inferior to 2 μm , which are hence not suitable for their direct implementation as catalytic microreactors in flow continuous processes, as the development of pressure drop is to be expected. It is furthermore important to underline, that the reported catalytic tests (catalytic cracking of large molecules) are not suited as here the shape selective properties of ZSM-5 play a minor role. Indeed, meso-/macroporous aluminosilica monoliths presented similar activity in such cracking reactions [37].

In the present study, we present the achievement of a ZSM-5 monolith (Si/Al ~ 40) with large homogeneous macropores (30 μm diameter), synthesized by pseudomorphic transformation of optimized aluminosilica monoliths using SAC conditions at 130 °C for 48 h. ZSM-5 monoliths were tested as catalytic flow microreactors in the alkylation of toluene by methanol to produce *para*-xylene with high selectivity.

2. Materials and methods

2.1. Synthesis of aluminosilica monoliths

Aluminosilica monoliths were synthesized using tetraethyl orthosilicate (TEOS), $\text{Al}(\text{NO}_3)_3 \cdot 9\text{H}_2\text{O}$, polyethylene oxide (PEO) of 100 kDa and HNO_3 (68 %) purchased from Sigma-Aldrich. The composition of the mixtures in molar ratio were: 1 Si: 0.61 EO Unit: 0.26 HNO_3 : x Al (NO_3)₃·9 H_2O : y H_2O . For Si/Al = 50, 30, 20, 10, 5, x = 0.02, 0.033, 0.05, 0.10, 2.20 and y = 14.21, 11, 9.5, 8, 6.4, respectively.

In a typical procedure of aluminosilica monolith synthesis (Si/Al = 30, x = 0.033 and y = 11), deionized water (19.012 g) was poured in 100 mL Erlenmeyer and (2.313 g) nitric acid (68 %) and (1.1885 g) Al (NO_3)₃·9 H_2O were added. The mixture was stirred for 5 min at room temperature. Polyethylene oxide (PEO) of 100 kDa (2.577 g) was added and stirred at room temperature until homogenization. The mixture was left at –19 °C for 15 min to cool down the solution without freezing. The Erlenmeyer was then placed in an ice bath and the solution was stirred. Tetraethyl orthosilicate (20 g), previously left 1 h at –19 °C, was directly added to the slurry and stirred for 30 min at 500 rpm to achieve a homogeneous mixture and a translucent solution. Polyvinyl chloride (PVC) tubes of 8 mm diameter and 10 cm length were closed on one side with a cap, sealed with parafilm and kept at –19 °C in the freezer. The tubes were taken from the freezer and filled with the mixture of the ice bath. The tubes were then closed by caps and sealed with parafilm, put horizontally in a rotating oven and left at 37 °C for 3 days. During this time, the phase separation and the sol-gel process took place to form the macroporous network of the monoliths. Then, the monoliths were removed from the molds and directly dried for 3 days at 60 °C at a relative humidity of 30 %. The monoliths were then calcined at 550 °C for 8 h with a heating rate of 2 °C min^{-1} from 25 to 550 °C under air to remove remaining PEO.

2.2. Synthesis of ZSM-5 monoliths

NaOH and tetrapropylammonium hydroxide (TPAOH) were purchased from Aldrich. An impregnation solution containing NaOH and TPAOH was prepared with the molar composition: $1000\text{H}_2\text{O}$: 1.55 NaOH: 4.74 TPAOH. Typically, an aluminosilica monoliths (Si/Al = 30 in the synthesis) of 2.5 cm length and 0.5 cm diameter (weight 310 mg)

was impregnated with 3 mL of the solution in a vial allowing a total immersion of the monolith and let for 20 h at 4 °C. The impregnated aluminosilica monolith was then placed on a steal net suspended in a stainless steel autoclave of 2.5 cm diameter with 4 mL of water previously added at the bottom. The autoclave was heated to 130 °C for 48 h. The monoliths were then washed with 200 mL of dionized water, dried at 60 °C overnight and calcined at 550 °C for 8 h (0.5 °C min⁻¹).

The acidic form of the ZSM-5 monolith was obtained by ionic exchange with an aqueous 0.1 M NH₄NO₃ solution (100 mL per g solid) at 90 °C under reflux for 1 h. The procedure was repeated 3 times with filtration in between, then washed with dionized water (100 mL per g solid), dried at 60 °C and calcined at 550 °C for 8 h to obtain the H⁺ form.

2.3. Materials characterization

X-Ray diffraction (XRD) patterns of the monoliths were performed using a Bruker D8 Advance diffractometer with a Bragg-Brentano geometry and equipped with a Bruker Lynx Eye detector. XRD patterns were recorded in the range 4–50° (2θ) to identify zeolite peaks. The angular step size was of 0.0197° and the counting time of 0.2 s per step.

The textural properties of the materials were determined from the N₂ adsorption/desorption isotherms at 77 K measured on a Micromeritics Tristar 3000 apparatus. The samples were previously outgassed in vacuum at 250 °C for 12 h. Micropore volumes of ZSM-5 were determined at p/p₀ = 0.1 when all micropores are filled.

Mercury porosimetry was carried out with a Micromeritics Autopore 9220 equipment by increasing the pressure from 0.0013 to 400 MPa. The mercury intrusion was performed with 100–300 mg of monolith of 0.5 cm diameter. Prior to the measurement the sample was outgassed at room temperature for 10 min. The meso- and macropore diameters were determined by the Washburn-Laplace equation (Eq. 1):

$$r = - \frac{2\gamma \cos \theta}{p_{int}} \quad (1)$$

with r the pore radius, θ the contact angle of mercury with the surface of the pore, γ the surface tension of mercury and p_{int} the pressure of intrusion. The mercury contact angle θ was set at 140° and the mercury surface tension γ at 0.485 N m⁻¹.

Monoliths morphology was studied using a Hitachi S-4800 I FEG-SEM Scanning Electron Microscope at "Plateau Technique de l'IEM laboratoire du Pole Chimie Balard Montpellier".

Energy Dispersive Spectroscopy (EDS) chemical analyses (in atomic %) were performed on a FEI Quanta 200 F (15 kV) apparatus. Molar ratio Si/Al and Na/Al of the ZSM-5 monolith was also calculated from ICP-OES analysis.

Acidity was probed with NH₃-TPD on a Micromeritics Autochem II with 50 mg of samples. For comparison with the ZSM-5 monolith, commercial ZSM-5 (Si/Al = 40) powder was purchased from Zeolyst International. This zeolite is composed of particles of 300–900 nm formed by an aggregation of spheres of 60–150 nm. For NH₃-TPD test, particles size of the commercial ZSM-5 powder was controlled by compressing (2 tons) for 1 min 200 mg of powder into pellets of 16 mm diameter with a press SPECAC 15 t and then grinding and sieving the pellets between 150 and 250 μm. The ZSM-5 monolith was crushed and sieved to reach 150–250 μm particles size. First, a 2 h calcination steps at 550 °C allows sample surface preparation before ammonia adsorption at 100 °C for 40 min with 5 % NH₃ in He. Desorption was carried out with a 25 cm³ min⁻¹ He flow at 10 °C min⁻¹ to 600 °C. Temperature ramping started when TCD signal was stable and desorption of weakly physisorbed ammonia finished. A calibration of TCD signal allowed data treatment and calculation of acid site concentration.

Determination of Brønsted and Lewis acidity was performed by FTIR/pyridine on a Nicolet 5700 instrument. The material was first compressed (0.5 ton) to form a self-supported pellet (2 cm⁻², 10–30 mg

and heated at 550 °C under air flow (60 mL min⁻¹). The sample was then outgassed (10⁻⁵ bar) at 200 °C for 1 h before to register the first FTIR spectrum. The sample was cooled at 150 °C and exposed to pyridine (1.5 mbar) for 5 min and outgassed (10⁻⁵ bar) to remove physisorbed pyridine. The quantification of Brønsted and Lewis acid sites was done by integration of the bands at 1545 and 1455 cm⁻¹, respectively, with the following extinction coefficients: ε₁₅₄₅ = 1.13 and ε₁₄₅₅ = 1.28 cm mol⁻¹.

²⁷Al MAS NMR spectra were registered with a VARIAN VNMRS600 spectrometer at 600 MHz ("wide bore" magnet of 14.1 T). A probe VARIAN T3 MAS was used. ZrO₂ rotors of 3.2 mm diameter were filled with crushed monolith powder and rotated at 22 kHz. The quantitative technique used a single pulse (π/6 of 2 μs) with ¹H decoupling and a recycling period of 1 s. The chemical shift was calibrated at 0 ppm with aluminum nitrate. The acquisition window was 192 kHz and a line broadening of 50 or 100 Hz was applied.

TGA was performed using PerkinElmer STA 6000 in order to determine the amount of tetrapropylammonium cations in as-synthesized ZSM-5 monolith. Ten milligrams of sample was heated from 40 to 900 °C with a heating rate of 10 °C min⁻¹ under air flow.

Mechanical stability of monoliths was evaluated in compression with an industrial test named "Brazilian test", "splitting tension test", "indirect tension test", or "indirect tensile strength test". The tests were realized with a tensile tester instrument Instron 3366. The cylindrical monolith of ~5 mm diameter and ~6 mm length was layed between two rigid parallel plates and a force (F) was applied with a crushing speed of 0.6 mm min⁻¹ until breaking at the crushing force (F_c). The force is expressed in Newton. The compressive strength (σ_c) was calculated by dividing F_c by the length (h) of the cylinder in mm and by πR, where R is the radius of the cylinder (in mm) with the following relationship to obtain σ_c in MPa:

$$\sigma_c = F_c / (\pi h R)$$

The average value of 3 measures (3 monoliths) was used to determine the compressive strength (σ_c) of the monolith.

2.4. Alkylation of toluene by methanol

ZSM-5 monolith and commercial ZSM-5 (Si/Al = 40) were used as catalysts. For packed-bed test, particles size of the commercial ZSM-5 powder was controlled by pressing 200 mg of powder into pellets of 16 mm diameter at 2 tons for 1 min with a press SPECAC 15 t and then grinding and sieving the pellets between 150 and 250 μm. For packed-bed test, the ZSM-5 monolith was crushed and sieved to reach 150–250 μm particles size. Toluene alkylation was carried out in a continuous gas flow fixed-bed reactor. Gas composition was evaluated by gas chromatography (GC-Agilent 7890 A equipped with a ZBWAX column of 30 m × 250 μm x 0.25 μm and a FID detector). In a typical packed-bed test, the reactor was filled with: 10 mg of catalyst previously mixed with 140 mg of quartz, and glass beads filling to the top. For direct use of ZSM-5 monolith, the monolith (0.5 cm diameter, 0.5 cm length, 37 mg) was inserted in a borosilicate tube of similar diameter (0.6 cm) and subjected to a flame allowing for a perfect adhesion of the monolith with the tube. After a preliminary 8 h calcination step at 550 °C under 40 mL min⁻¹ air flow, the temperature was set at 350 °C flowing N₂. 0.020 mL min⁻¹ of liquid toluene and methanol in the desired ratio were fed using a HPLC pump (Jasco PU-4180) and mixed with 80 mL min⁻¹ N₂. GC separation program allowed separation of light hydrocarbons, methanol (M), benzene (B), toluene (T), *para*-/*meta*-/*ortho*-xylene (X) isomers and trimethylbenzene (TMB). Conversion and selectivity were calculated according to the following equations, using the molar quantity of each compound determined from the peak area in the chromatogram.

$$\text{Toluene conversion : } C_T = \frac{B + X + TMB}{T + B + X + TMB} \times 100 (\%)$$

$$\text{Methanol conversion} : C_M = \frac{M_0 - M}{M_0} \times 100$$

$$\text{Xylene isomers selectivity} : S_{i-x} = \frac{i - X}{\sum i - X} \times 100 (\%)$$

where i = p- or m- or o-

$$\text{Aromatic selectivity} : S_p = \frac{P}{\sum P} \times 100 (\%)$$

where p = B or X or TMB

$$\text{p-xylene yield} : R_{p-x} = C_T \times S_X \times S_{p-x} (\%)$$

3. Results and discussion

3.1. Aluminosilica monoliths

Most of the aluminosilica monoliths presented in literature feature high amount of alumina (Si/Al = 7) [38–41], except for the synthesis proposed by Zhao et al. [35] and Yang et al. [37] ($10 < \text{Si/Al} < 100$), suitable for ZSM-5 synthesis. The synthesis of aluminosilica monoliths developed by Yang et al. [37] are of great interest as they evidenced that to generate a suitable phase separation, *i.e.* spinodal decomposition, the addition of $\text{Al}(\text{NO}_3)_3 \cdot 9\text{H}_2\text{O}$ in the synthesis mixture should be compensated by a decrease of the water content, otherwise the phase separation occurs much faster than the sol-gel transition and the macropore morphology turns from bicontinuous domains to spherical particle aggregates. They used a dual templating approach with triblock copolymer (P123) and PEO (10 kDa) to produce hierarchical meso-/macroporous aluminosilica monoliths of $700 \text{ m}^2 \text{ g}^{-1}$ featuring $7 \mu\text{m}$ macropore diameter and 5.6 nm mesopore diameter (reaction temperature of 60°C for 24 h).

In the present study, different synthesis conditions were used: absence of P123, using a longer PEO chain (100 kDa) and a lower temperature (37°C). We have analyzed the effect of aluminum addition and its compensation by a decrease of water content in the gel composition. Without modification of water amount, only aluminosilica monoliths synthesized with $\text{Si/Al} \geq 50$ are stable and showed a

bicontinuous phase of the macropore network. For higher added alumina amounts in the synthesis gel ($5 < \text{Si/Al} < 50$) the amount of water required to be decreased, in order to achieve a bicontinuous macropore network. We found that, to insure a bicontinuous domains, the composition of the gel in molar ratio (1 Si: 0.61 EO Unit: 0.26 HNO_3 : x $\text{Al}(\text{NO}_3)_3 \cdot 9\text{H}_2\text{O}$: y H_2O) should follow a linear relationship of the molar ratio x and y (Eq. (2)):

$$y = 0.166 (1/x) + 5.99 \quad [2]$$

A further important aspect in the synthesis procedure is to place the tubes horizontally in the oven and to automatically rotate them during the entire sol-gel process to insure a homogeneous repartition of Al within the whole aluminosilica monolith.

The aluminosilica monoliths feature homogeneous macropores of ca. $30 \mu\text{m}$ diameter and a skeleton thickness of $25\text{--}30 \mu\text{m}$ (Fig. 1). They present a hierarchical micro-/macroporosity with a micropore volume of ca. 0.28 mL g^{-1} as revealed by nitrogen sorption isotherm at 77 K and a macropore volume of ca. 0.87 mL g^{-1} as evaluated by Hg porosimetry (Fig. 1, Table 1). The microporous volume of aluminosilica monoliths is due to the polymeric structure of the silica network doped with aluminum with a low condensation state of the species, which is typical for sol-gel synthesis in acidic medium. Similar micropore volume 0.35 mL g^{-1} and specific surface area ($630 \text{ m}^2 \text{ g}^{-1}$) were obtained for pure silica monolith after the acidic synthesis (without additional basic treatment) [42]. Aluminosilica monoliths are amorphous as showed by the XRD pattern, presenting a large bump at $2\theta = 20^\circ$ (Fig. 2). Although no washing was performed after the synthesis, the amount of aluminum incorporated in the final aluminosilica monoliths was found to be slightly inferior to the aluminum present in the synthesis gel (Table 1). The information derived from ^{27}Al MAS NMR spectra allowed to conclude that the majority of aluminum is in tetrahedral environment (intense peak at 52 ppm) and a minor part in octahedral environment (large distribution around 0 ppm and a very narrow signal at -1 ppm) (Fig. 3).

3.2. ZSM-5 monoliths

Aluminosilica monoliths were impregnated with a mixture of a molar composition of $1000\text{H}_2\text{O}$: 1.55 NaOH: 4.74 TPAOH and subjected to SAC

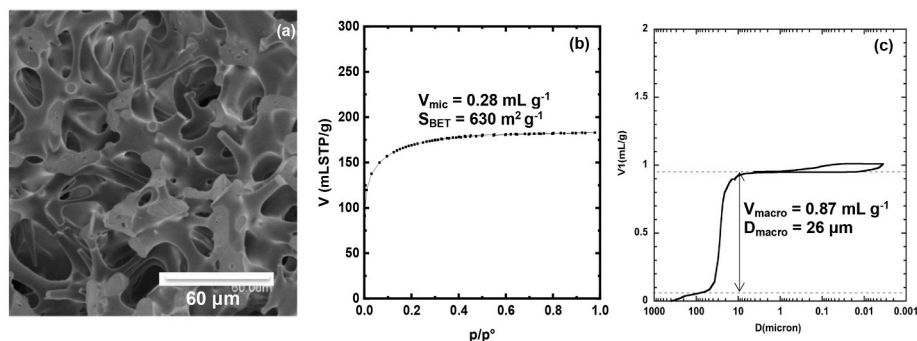


Fig. 1. (a) SEM image, (b) nitrogen sorption isotherm at 77 K and (c) Hg porosimetry of aluminosilica monoliths (Si/Al = 30 in the synthesis mixture). Macropore volume of the monolith is determined after the compressibility zone (dashed line at low pore volume).

Table 1
Properties of aluminosilica monoliths.

Si/Al synthesis gel	Si/Al monolith EDS	$S_{\text{BET}}^a \text{ m}^2 \text{ g}^{-1}$	$V_{\text{mic}} \text{ mL g}^{-1}$	$D_{\text{macro}} \mu\text{m}$	$e_{\text{skeleton}} \mu\text{m}$	$V_{\text{macro}} \text{ mL g}^{-1}$
10	27	721	0.33	–	–	–
20	32	605	0.28	30	25	–
30	38	625	0.27	26 ^b	30	0.87 ^b
50	50	640	0.29	25	25	–

^a BET surface areas were determined considering Rouquerol criteria [43].

^b Determined by Hg porosimetry. The other values of macropore diameter are determined from SEM pictures.

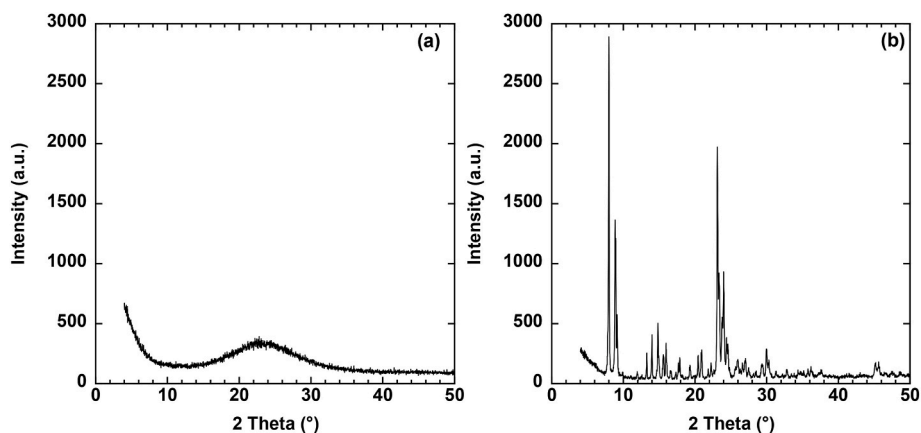


Fig. 2. XRD of (a) aluminosilica monolith and (b) ZSM-5 monolith(A).

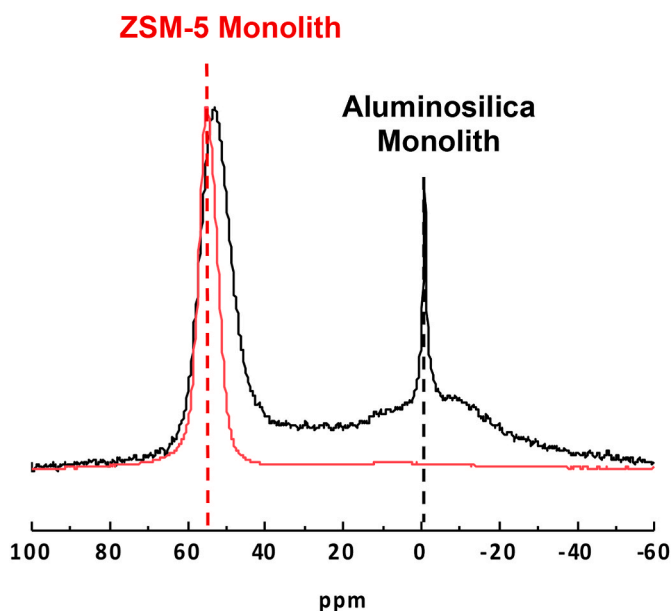


Fig. 3. ^{27}Al MAS NMR of (black) aluminosilica monolith ($\text{Si}/\text{Al} = 30$ in the synthesis gel) and (red) ZSM-5 monolith(A).

treatment at $130\text{ }^\circ\text{C}$ for 48 h. The composition of this solution is close to the one ($1000\text{H}_2\text{O}$: 1.58 NaOH: 4.74 TPAOH: 1.58 $\text{Al}(\text{OiPr})_3$) initially proposed by the group of Zhao [30] in 2006 to synthesize ZSM-5 monoliths (absence of distinguishable crystals, low micropore volume of 0.09 mL g^{-1}) from silica monoliths, except the absence of aluminum source as this is provided by the composition of the aluminosilica monolith itself.

It was found that the Si/Al ratio used in the synthesis of the pristine monolith plays a fundamental role in achieving a stable ZSM-5 monolith. Too high Si/Al ratios ($\text{Si}/\text{Al} > 30$) allowed only to achieve partially or totally dissolved monolith fragments. With too low Si/Al ratios ($\text{Si}/\text{Al} = 20$), aluminosilica monoliths were not transformed under the applied conditions. Increasing aluminum content allowed to stabilize the aluminosilica monolith against the dissolution and an optimum of Si/Al ratio needs to be identified for a given alkaline medium in order to adapt the aluminosilicate dissolution rate to ZSM-5 crystallization the rate (pseudomorphic transformation principle [44]). In the applied conditions, only the pristine aluminosilica monolith synthesized with a Si/Al ratio of 30 could be successfully transformed into a stable ZSM-5 monolith. From the XRD pattern only peaks corresponding to the MFI structure and the absence of amorphous phase can be observed (Fig. 2).

The nitrogen sorption isotherm (Fig. 4) confirmed the full transformation into ZSM-5, allowing to calculate a micropore volume and a BET surface area of 0.163 mL g^{-1} and $382\text{ m}^2\text{ g}^{-1}$, respectively, which are in agreement with the theoretical values for MFI structure ($V_{\text{mic}} = 0.157\text{ mL g}^{-1}$, $S_{\text{BET}} = 393\text{ m}^2\text{ g}^{-1}$) [43]. Aluminum was perfectly incorporated into the zeolite framework, as evidenced by ^{27}Al MAS NMR (Fig. 3), which allows to observe the presence of a signal at 54 ppm, characteristic of a tetrahedral environment.

SEM images allow for inferring a network of homogeneous macropores of $24\text{--}26\text{ }\mu\text{m}$ (Fig. 4) for the ZSM-5 monolith, similar as for the pristine aluminosilica monolith (Fig. 1). From Hg porosimetry, the same macropore diameter and identical primary macropore volume of 0.87 mL g^{-1} for both ZSM-5 and aluminosilica monoliths could be calculated (Fig. 1, Table 1). A secondary step in mercury intrusion could be detected in the ZSM-5 monolith corresponding to a macropore diameter of $4\text{ }\mu\text{m}$ and a macropore volume of 0.25 mL g^{-1} (Fig. 4). The secondary macroporosity results from the Hg intrusion into interparticular voids resulting from the 3D aggregation of spherical particles of $3\text{--}6\text{ }\mu\text{m}$ diameter as evidenced by SEM images. The SEM images further allow for visualizing that the particles themselves are composed of thin plate-like shaped crystallites. It is reasonable to assume that the crystallites and the particles are connected through hydrogen bonds, as it is known that plate-like MFI crystals offer a maximum of (010) planes, which surface energy was shown to be the most propitious to bonding between crystals [45]. Slight modifications on the composition of the solution used to impregnate aluminosilica monoliths allow to achieve ZSM-5 monoliths with similar textural properties, except for ZSM-5 monolith(D) (Table 2). It is interesting to note that when the amount of TPAOH was halved a ZSM-5 monolith was obtained with no secondary macroporosity due to the formation of particles twice as large ($12\text{ }\mu\text{m}$ diameter) with more distinguishable plate-shaped crystallites (Fig. 5). Indeed, TPA^+ is known to act as both crystal growth inhibitor and organic structure directing agent (OSDA) to induce the formation of crystals [46]. It is possible to assume that TPA^+ adsorbs on the negatively charge surface of the aluminosilica monolith during the impregnation period. Then, when temperature is increased for the crystallization step, the crystal growth occurs rapidly on the surface of aluminosilica monolith in the vicinity of TPA^+ . A higher amount of TPA^+ would then lead to a large number of nuclei and consequently to smaller crystals. Differently, by reducing the amount of TPA^+ less nuclei would develop, leading to the formation of larger crystals.

For catalytic applications in continuous flow with full monoliths, ZSM-5 monoliths of type A, B, C and E featuring a secondary macroporosity should be preferred, as it was previously reported for other kind of zeolitic monoliths (LTA [26] and FAU-X [28]) that an equal accessibility to the active sites was reached only if a secondary macroporosity was present. Indeed, perfect breakthrough curves with vertical slope

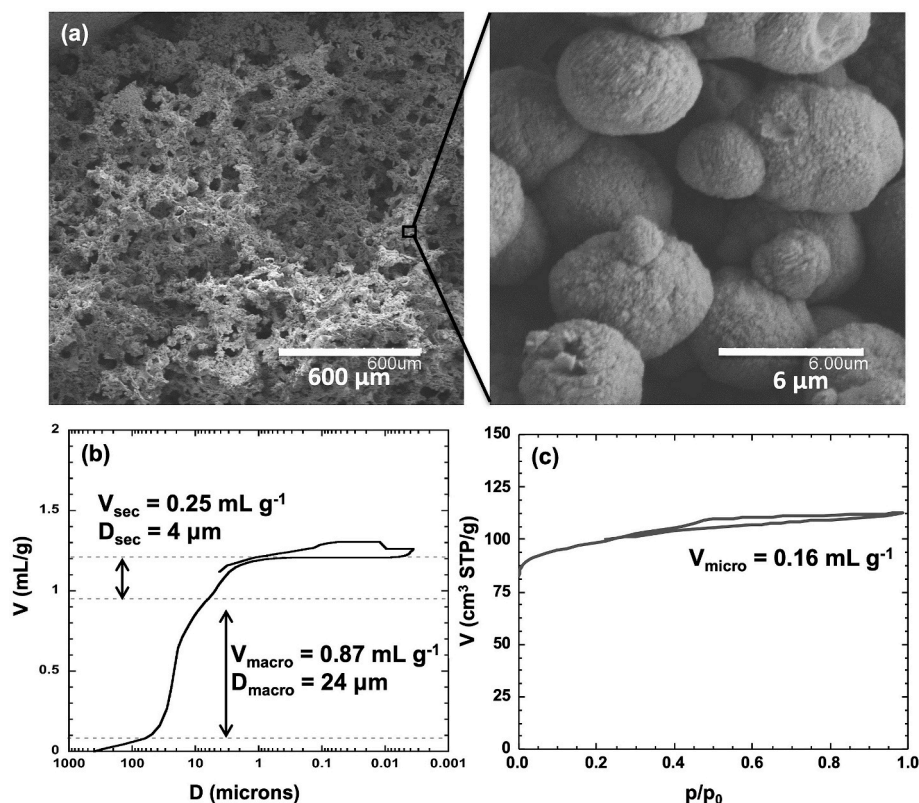


Fig. 4. (a) SEM images, (b) Hg porosimetry and (c) nitrogen sorption isotherm at 77 K of ZSM-5 monolith(A). Macropore volume of the monolith is determined after the compressibility zone (dashed line at low pore volume).

Table 2

Properties of full ZSM-5 monoliths as a function of molar composition of the impregnation mixture.

ZSM-5 Monolith	Mixture molar composition			V_{mic}^a mL g ⁻¹	S_{BET}^b m ² g ⁻¹	S_{ext}^a m ² g ⁻¹	V_{macro}^c mL g ⁻¹	$V_{sec}^{c,d}$ mL g ⁻¹	D_{macro}^c μm	$D_{sec}^{c,d}$ μm
	H ₂ O	NaOH	TPAOH							
A	1000	1.55	4.74	0.163	382	19	0.87	0.25	24	4.0
B	1000	2.36	4.74	0.150	353	26	1.11	0.32	33	4.8
C	1000	1.55	5.93	0.175	405	21	1.01	0.29	28	4.1
D	1000	1.55	2.37	0.170	408	24	1.09	no	45	no
E	1000	2.08	6.32	0.176	409	28	0.87	0.21	25	2.9

^a Determined by t-plot analysis [43].

^b BET surface areas determined considering Rouquerol criteria [43].

^c Determined by Hg porosimetry.

^d Secondary macroporosity induced between large particles of crystallite aggregates.

were obtained for the capture of cations (Sr²⁺, Cs⁺) only with zeolite monoliths featuring a secondary macroporosity between crystals, while a breakthrough curve with leakage (bent slope) was observed for zeolite monoliths featuring larger crystals and absence of secondary macroporosity [26].

The composition of calcined ZSM-5 monolith(A) was measured locally by EDS on different locations of the monolith cross-section (0.4 cm diameter). The average values of molar ratios are Na/Al = 2.09 ± 1 and Si/Al = 44.06 ± 3. The composition is uniform throughout the cross-section. Elemental analysis determined by ICP-OES after alkaline fusion (NaOH and KNO₃ at 600 °C) to measure the Si content and after acidic dissolution (HNO₃ and HF at 200 °C) to measure the Na and Al contents confirmed the molar ratios inferred by EDS (Na/Al = 1.64 and Si/Al = 41). This corresponds to a composition of 12.8, 0.31 and 0.51 mmol for Si, Al and Na g⁻¹, respectively. The Si/Al ratio of ZSM-5 monolith(A) (Si/Al = 41) is closed to the initial Si/Al ratio of the aluminosilica monolith (Si/Al = 38) used for its synthesis (Table 1). The amount of Na species in ZSM-5 monolith(A) is larger than that of Al

atoms. This indicates that in addition to Na⁺ counterbalancing tetrahedrally coordinated Al located within the channels, known to promote *para*-xylene selectivity after its exchange by H⁺ [47], the excess of Na allows for neutralize negative charged hydroxyls (Si-O⁻). The latter are most probably located on the external surface of ZSM-5 crystallites.

The incorporation of TPA⁺ within as-synthesized ZSM-5 framework was further investigated. Indeed, it is known that TPA⁺ occludes in the channel intersections (~0.8 nm) and hence confers an energetic preferential position of Al close to N⁺ centers in these intersections [47,48]. Hence, after calcination the resulting protons will be located in the channel intersections and would not lead to an enhancement of the *para*-xylene selectivity in opposite to those located within the channels [47]. From the TGA on as-synthesized ZSM-5 monolith(A) a sharp weight loss of 9.43 % between 345 and 520 °C can be observed, which can be assigned to the degradation of TPA, which corresponds to 10.93 % of the remaining mass at 600 °C (calcined ZSM-5). It can hence be calculated that 0.59 TPA⁺ mmol g⁻¹ are present in the as-synthesized ZSM-5 monolith, corresponding to a TPA/Al ratio of 1.89. The amount

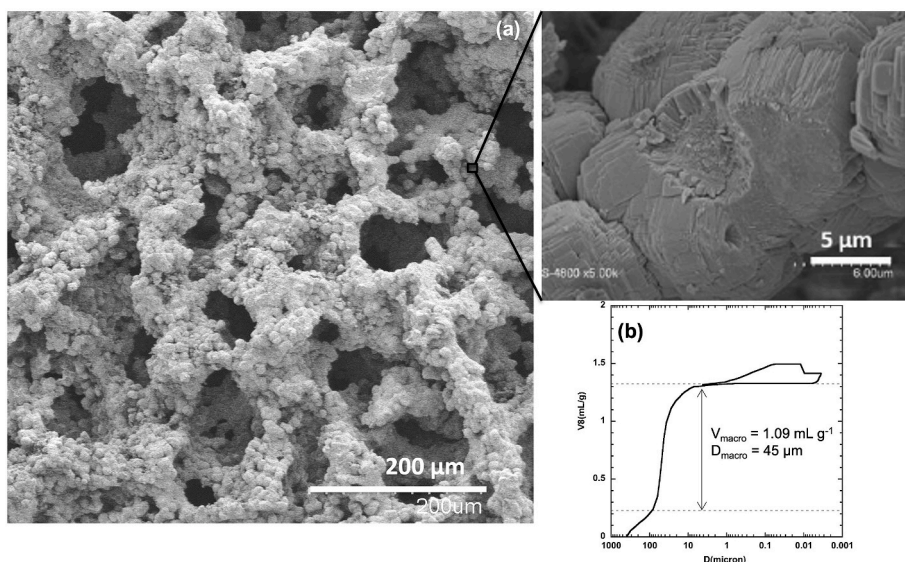


Fig. 5. (a) SEM images and (b) Hg porosimetry of ZSM-5 monolith(D). Macropore volume of the monolith is determined after the compressibility zone (dashed line at low pore volume).

of TPA species is larger than that of Al atoms in ZSM-5 monolith(A). It was reported in the literature that for exceeding amounts of TPA^+ ($2.19 < \text{TPA}/\text{Al} < 2.26$) in as-synthesized ZSM-5 the TPA^+ would occupy all of the channel intersections of the zeolite framework [47]. Moreover, it is known that TPA^+ promotes the formation of silanol/siloxy defects ($\text{SiO}^- \dots \text{HOSi}$) in zeolite framework [49], which can be healed after calcination. The total amount of compensating cations in as-synthesized ZSM-5 monolith(A) is $(\text{Na} + \text{TPA})/\text{Al} = 3.53$, similar to what was previously reported [47]. Hence, in the calcined ZSM-5 monolith(A), it is possible to predict that Na^+ cations are within the channels and on the external surface of the ZSM-5 crystallites as compensating cations of the zeolite framework and of the negative charge hydroxyls ($\text{Si}-\text{O}$). It is further possible to conclude that the H^+ resulting from TPA^+ decomposition are located in the channel intersection as compensating cations of the zeolite framework. The Na^+ present in the channels were exchanged by NH_4^+ followed by a calcination in order to achieve H^+ -ZSM-5 monolith used in the catalytic experiment. The particular behavior of ZSM-5 zeolites in catalysis is due to their strong Brønsted

acidity given by bridging protons $\text{SiO}(\text{H}^+)\text{Al}$. From EDS measurements on cross-section of the H^+ -ZSM-5 monolith identical Si/Al composition was monitored ($\text{Si}/\text{Al} = 43 \pm 3$). Na could not be detected, indicating the full exchange with H^+ . The number of acid sites was measured by NH_3 -TPD (Fig. 6) and by FTIR-pyridine (Table 3) and compared to the acidity of a commercial ZSM-5 with similar Si/Al ratio ($\text{Si}/\text{Al} = 40$). NH_3 -TPD analyses of H^+ -ZSM-5 monolith and commercial ZSM-5 (Fig. 6) features two contributions, a low temperature peak at 200°C corresponding to NH_3 desorption from weak acid sites or from NH_3 interacting with NH_4^+ cations by solvation phenomenon [50]. The latter can lead to an overestimation of the number of weak acid sites. A high temperature peak centered at 420°C is further observed, characteristic of the desorption of NH_3 from strong acid sites in ZSM-5 zeolites. The H^+ -ZSM-5 monolith(A) ($\text{Si}/\text{Al} = 43$) features a total number of acid sites concentration of 0.32 mmol g^{-1} , of which 0.13 mmol g^{-1} corresponds to strong acid sites. The commercial ZSM-5 sample ($\text{Si}/\text{Al} = 40$) features a slightly higher amount of acid sites with a total of 0.43 mmol g^{-1} , including 0.21 mmol g^{-1} of strong acid sites. The peak at high temperature is generally associated to Brønsted acidity for most zeolites [51,52]. However, it has been proposed that in certain zeolites, such as ZSM-5, in addition to NH_4^+ mono-coordinated by strong H-bonding with the basic oxygen of the zeolite network, bi- or tri-coordinated NH_4^+ could exist that possibly underestimate the number of strong acid sites [50].

FTIR/Pyridine analysis was performed to confirm the nature of the acid sites observed by NH_3 -TPD. For the H^+ -ZSM-5 monolith ($\text{Si}/\text{Al} = 43$) catalyst and commercial ZSM-5 ($\text{Si}/\text{Al} = 40$), typical bands at 1545 and 1455 cm^{-1} were observed in the FTIR spectra, resulting from the adsorbed pyridinium ions on Brønsted acid sites (BAS) and pyridine coordinated to Lewis acid sites (LAS), respectively. A very low concentration of LAS is observed (0.03 mmol g^{-1}) (Table 3). The BAS concentrations in H^+ -ZSM-5 monolith(A) ($\text{Si}/\text{Al} = 43$) and in commercial ZSM-5 ($\text{Si}/\text{Al} = 40$) are of 0.14 and 0.20 mmol g^{-1} , respectively, in agreement with the number of strong acid sites found by TPD- NH_3 (0.13 and 0.21 mmol g^{-1} , respectively) (Table 3). This confirms that the high temperature peak in TPD- NH_3 for ZSM-5 materials is corresponding to BAS as for most zeolites [51,52]. The high concentration of weak acid sites (0.19 and 0.22 mmol g^{-1} , respectively) found by NH_3 -TPD results presumably from the solvation by NH_3 of already formed NH_4^+ [53] as it cannot be ascribed to LAS present in very low concentration (0.03 mmol g^{-1}) (Table 3). The BAS concentration of H^+ -ZSM-5 monolith (0.14 mmol g^{-1}) measured by FTIR/Pyridine is slightly lower than the one expected for a ZSM-5 with a Si/Al ratio of 43 taking into account the

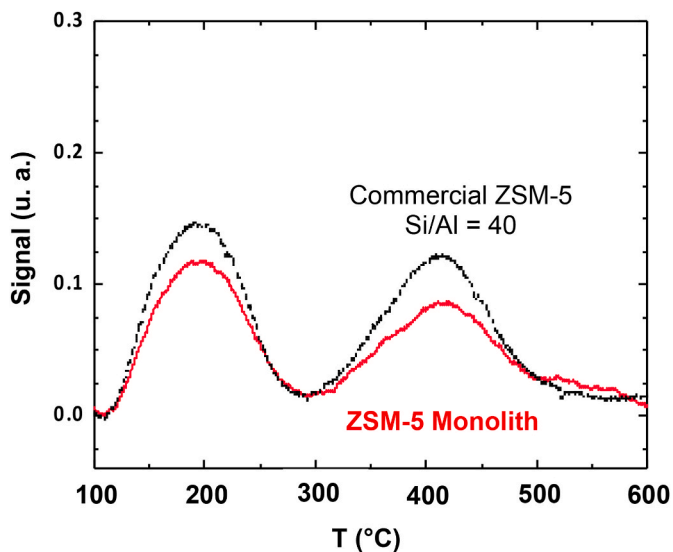


Fig. 6. NH_3 TPD of (red) H^+ -ZSM-5 monolith(A) and (black) commercial H^+ -ZSM-5 powder ($\text{Si}/\text{Al} = 40$).

Table 3

Acidity of ZSM-5 monolith compared to commercial ZSM-5 (Si/Al = 40).

Catalysts	S_{BET} $\text{m}^2 \text{g}^{-1}$	$S_{\text{ext}}^{\text{a}}$ $\text{m}^2 \text{g}^{-1}$	TPD-NH ₃			FTIR-Pyridine		
			Weak mmol g ⁻¹	Strong mmol g ⁻¹	Total mmol g ⁻¹	Brønsted mmol g ⁻¹	Lewis mmol g ⁻¹	Total mmol g ⁻¹
ZSM-5 Monolith(A)	382	19	0.19	0.13	0.32	0.14	0.03	0.17
ZSM-5 (Si/Al = 40)	445	55	0.22	0.21	0.43	0.20	0.04	0.24

^a Determined by t-plot analysis [43].

relationship between BAS and tetrahedral aluminum species in ZSM-5 [54]:

$$\text{BAS (mmol/g)} = 7.28 [\text{Al}/(\text{Al} + \text{Si})]$$

Indeed, ZSM-5 with a ratio Si/Al = 43 should feature a BAS concentration of 0.16 mmol g⁻¹. The slightly lower concentration of BAS (0.14 mmol g⁻¹) found for H⁺-ZSM-5 monolith could result of a lower accessibility of pyridine, possibly due to the stacking of the plate-like crystallites, inducing mass transfer limitations. Another explanation could be that some Al tetrahedral are not incorporated in the MFI framework and could serve as binder between ZSM-5 particles. A BAS concentration of 0.14 mmol g⁻¹ corresponds to a ZSM-5 with a ratio Si/Al = 52 and hence, 0.064 mmol g⁻¹ of Al over 0.310 mmol g⁻¹ could not be incorporated in the zeolite framework.

The mechanical stability of ZSM-5 monoliths was measured using an industrial test named “Brazilian tensile strength” test or “indirect tension” test, *i.e.* with the cylindrical monolith laying on its length (Fig. 7). It is to note that the use of this configuration features advantages over the uniaxial compression test (cylinder placed perpendicular to the plate), as the latter requires strict adherence of the sample and sophisticated testing techniques. The compression strength of ZSM-5 monolith was compared to the one of the pristine aluminosilica monolith. At the compression force F_c , both monoliths break in the middle perpendicularly to the force resulting in two identical parts (Fig. 7). According to the “Brazilian” test, this demonstrates that the monoliths are homogeneous, elastic and isotropic materials. The compression strength of ZSM-5 monolith(A) is $\sigma_c = 0.30$ MPa for a density of 0.523 g cm⁻³ and a porosity of 65.85 % (74.38 % with the microporosity). For the aluminosilica monolith σ_c was 1.71 MPa for a density of 0.583 g cm⁻³ and a porosity of 58.78 % (74.15 % with the microporosity). Densities and porosities (without microporosity) were determined by Hg porosimetry. It is known that the mechanical strength is strongly dependent of the mesoscopic structure [55]. Hence, the lower compressive strength of ZSM-5 monolith compared to aluminosilica monolith is probably due to the existing secondary macroporosity in ZSM-5 monolith(A), leading to a lower density and a higher porosity. Mechanical stabilities of porous materials are also dependent from their bulk mechanical stability [55].

Indeed, it is possible to assume that bulk amorphous aluminosilica presents a higher elasticity than bulk crystalline ZSM-5, leading to higher mechanical strength of their porous forms.

3.3. Alkylation of toluene by methanol with ZSM-5 monoliths

Zeolites exhibit high performance in many acidic catalytic reactions thanks to their shape selective properties, strong acidity and thermal stability. Their properties can be finely tuned by modification of the composition, crystal morphology and external surface acidity. A relevant example is toluene alkylation with methanol to produce *para*-xylene; a major intermediate used to produce high-value polymers. Medium pore zeolites, such as ZSM-5, are the most suitable catalysts for toluene alkylation [4]. The main reaction product is *para*-xylene, but it is accompanied by its isomerization into *ortho*- and *meta*-xylenes. Moreover, side reactions such as toluene disproportionation into benzene and xylenes, transformation of methanol into light hydrocarbons and poly-methylation of toluene in trimethylbenzenes can arise (Scheme 1).

Because of its linear shape, *para*-xylene diffuses more rapidly than *ortho*- and *meta*-xylenes in the channels of ZSM-5, but isomerization of *para*-xylene into *ortho*- and *meta*-xylenes generally occurs on the acid sites present on the external surface of the crystals, leading in most of the case to the thermodynamic equilibrium composition of *para*-/*meta*-/*ortho*-xylene of 24: 52: 24 % [5]. The shape-selective capability of ZSM-5 to produce *para*-xylene from toluene alkylation continues to be one of the industrial challenges. There are different strategies to design highly selective ZSM-5 [5].

- Passivation of the external acid sites to prevent xylene isomerization or unselective toluene methylation reactions [56–59].
- Inverting Al gradient concentration in the crystal to present very low Al concentration on the external surface [6].
- Tuning crystal shape to maximize the pore openings through sinusoidal channels [6].
- Increasing the crystal size (10 μm) to lengthen the diffusion pathway of *ortho*- and *meta*-xylenes to maximize their diffusion resistance [60, 61].

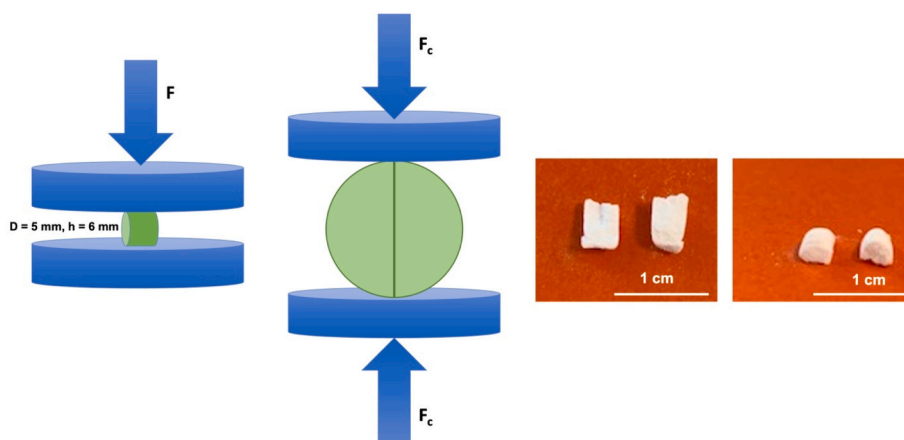
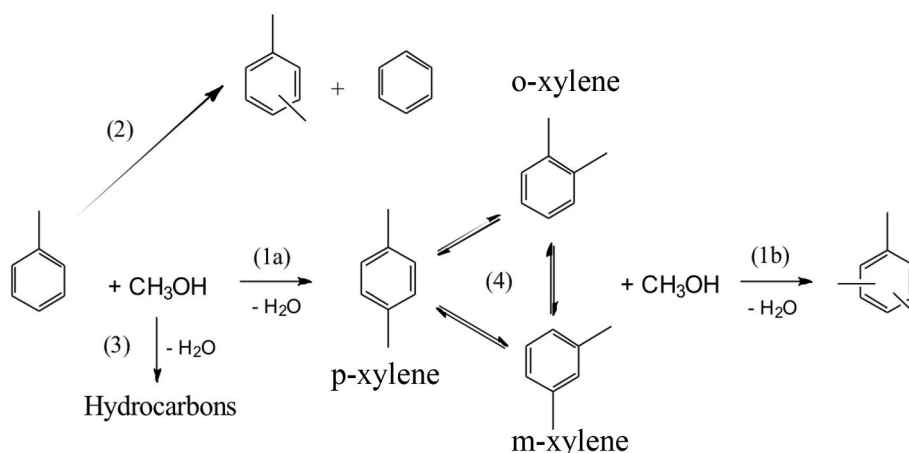


Fig. 7. Schematic representation of the “Brazilian tensile strength” mechanical test. At the compression force (F_c) monolith breaks along the axis perpendicular to the plate. Images of ZSM-5 monolith(A) after breaking.



Scheme 1. Main reactions involved in the alkylation of toluene by MeOH. (1a) Toluene alkylation; (1 b) xylenes alkylation; (2) toluene disproportionation; (3) methanol to hydrocarbons; (4) xylenes isomerization.

- Lowering the contact time to limit the isomerization [62].

It was also proposed to introduce mesopores in ZSM-5 crystals to increase para-xylene diffusion [63]. However, we have previously demonstrated that this strategy was not efficient as this reaction is not diffusion limited [64]. The reaction conditions were chosen in order to maximize the xylenes yield, to limit the formation of side products and above all to avoid thermodynamic equilibrium of the *para*-/*meta*-/*ortho*-xylenes, *i. e.* a short contact time of 0.03 s, a temperature of 350 °C and a toluene/MeOH ratio of 4 corresponding to a theoretical upper limit of toluene conversion of 25 % [64]. These conditions allowed for achieving very high selectivity (90 %) in xylenes and very low selectivity (10 %) in side products (trimethylbenzenes) using mesoporous ZSM-5 featuring cubic nanocrystals of 150 nm. The toluene and methanol conversion increased with rising BAS concentration in ZSM-5 catalysts, independently of the presence of mesopores, prior to reach a plateau for ZSM-5 featuring BAS of 0.25 mmol H⁺ g⁻¹, corresponding to a maximum of 10 % conversion of toluene with a methanol efficiency of 90 %. At short contact times, ZSM-5 should be highly active, *i.e.* containing high BAS concentration to balance the toluene conversion loss due to the limited time for toluene to enter into the pores of the zeolite. The selectivity into *para*-xylene increased slightly from 49 to 61 % with increasing BAS concentration from 0.16 to 0.47 mmol H⁺ g⁻¹, respectively, whereas *ortho*-xylene (the largest isomer) selectivity decreased from 23 to 14 % and *meta*-xylene selectivity remained roughly constant ~26 % [64]. Due to low contact time, *para*-xylene selectivity was above thermodynamic equilibrium (>24 %).

Numerous reaction conditions were reported for the toluene alkylation (different temperatures, pressures, contact times, toluene/MeOH ratios, amount of acid site concentration, addition of H₂O and/or H₂ at different volumes and flow rates, ...) [6], hence the direct comparison between literature results is often difficult. For ZSM-5 monoliths, in order to examine the influence of their unique crystal morphology (a 3D aggregation of spherical particles of ~6 μm composed of thin plate-like crystallites), the same conditions as our previous work were chosen

[64]: contact time of 0.03 s driven by N₂ flow rate of 80 mL min⁻¹, a temperature of 350 °C and a toluene/MeOH ratio of 4. No addition of H₂O or H₂ is used.

First, H⁺-ZSM-5 monolith(A) (Si/Al = 43) was tested in a packed-bed reactor as crushed and sieved fractions. The achieved results (Table 4) were compared to those obtained with a packed-bed filled with commercial ZSM-5 (Si/Al = 40). The commercial ZSM-5 (Si/Al = 40) features a higher toluene conversion of 7 % in accordance with its higher BAS concentration [64] of 0.20 mmol H⁺ g⁻¹ and an expected *para*-xylene selectivity of 53 %. ZSM-5 monolith presents a lower toluene conversion of 3 %, in accordance with its lower BAS concentration [64] (0.14 mmol H⁺ g⁻¹) and, remarkably, a much higher *para*-xylene selectivity of 68 %. Indeed, for such BAS concentration a selectivity of 48 % was expected [64].

In literature three hypothesis could explain the achieved *para*-xylene selectivity by the ZSM-5 monoliths: (i) a low external surface area with very low concentration of Al and hence BAS [6], (ii) the maximization of pore openings through sinusoidal channels [6] and (iii) the pore-confinement effect with Al (and associated H⁺) location preferentially inside the channels [48]. As far as the latter is concerned, reported experiments with similar toluene conversion from 1 to 3 % [48] as for ZSM-5 monoliths indicated that when Al was located in the channel intersections the *para*-xylene selectivity was 25 %, whereas it reached 75 % when Al was located inside the channels. By DFT calculations, they calculated the Gibbs free energy barriers of xylenes formation transition states. For Al located in channel intersections, toluene methylation occurred with effective barriers of 123, 132, 125 kJ mol⁻¹ for *para*-, *meta*-, *ortho*-xylenes, suggesting a similar preference for *para*- and *ortho*-xylene formation, and selectivity of 25, 10, 65 % were achieved, respectively. For Al located within the channels, higher toluene methylation barriers were found with 149, 152, 172 kJ mol⁻¹ for *para*-, *meta*-, *ortho*-xylenes, suggesting a strong preference for *para*-over *ortho*-xylene formation due to confinement effects, and selectivity of 75, 5, 20 % were achieved for *para*-, *meta*-, *ortho*-xylenes, respectively. Higher *para*-xylene selectivity (75 %) and lower rate of reaction were

Table 4

Catalytic results of toluene alkylation by methanol over H⁺-ZSM-5 monoliths and commercial H⁺-ZSM-5 (Si/Al = 40).

Catalysts	Contact time s	Conv. Toluene %	Conv. MeOH %	Sel. TMB %	Sel. Xylenes %	<i>para</i> -xylene %	<i>meta</i> -xylene %	<i>ortho</i> -xylene %
H ⁺ -ZSM-5 commercial Si/Al = 40 (packed-bed)	0.03	7	65	11	89	53	26	21
H ⁺ -ZSM-5 Monolith(A) grinded (packed-bed)	0.03	3	50	8	92	68	17	15
H ⁺ -ZSM-5 Monolith(A) (microreactor) ^a	0.07	1	46	8	92	81.4	9.3	9.3

^a Full monolith 0.5 cm diameter, 0.5 cm length, 37 mg.

therefore obtained when Al (and associated H⁺) were located within channels. This was also further demonstrated by using other zeolites, such as TON, a one-dimensional zeolite with a micropore diameter (0.46 × 0.57 nm) similar to that of ZSM-5 sinusoidal channels (0.51 × 0.55 nm), and beta a three-dimensional zeolite with a micropore diameter (0.76 × 0.64 nm) similar to that of ZSM-5 channel intersections (~0.8 nm). The selectivity in *para*-xylene was 80 % and 30 % for TON and beta, respectively, confirming the preferential selectivity in *para*-xylene if Al (and associated H⁺) is located within the channels rather than in channel intersections. In the case of the present ZSM-5 monolith the Al (and associated H⁺) should be located in both channel intersections and inside the channels (as both TPA⁺ and Na⁺ were found in the material) and hence no preferential *para*-xylene formation over *ortho*-xylene should be observed.

The commercial ZSM-5 (Si/Al = 40) is composed of spherical particles of 300–900 nm presenting an aggregation of round/cubic nanoparticles of 60–150 nm, leading to an external surface area of 55 m² g⁻¹ for a total BET surface area of 445 m² g⁻¹ (Table 3). As its total BAS concentration is 0.20 mmol H⁺ g⁻¹, the acidity on external surface area would hence be equal to 0.025 mmol H⁺ g⁻¹. The external surface area of ZSM-5 monolith(A) is 19 m² g⁻¹ for a total BET surface area of 382 m² g⁻¹ (Table 3), hence the acidity on external surface area would be equal to 0.007 mmol H⁺ g⁻¹. Hence, the ZSM-5 monolith exhibits 3 times less protons on the external surface compared to commercial ZSM-5, which could explain the lower amount of side reactions as isomerization of *para*-xylene into *ortho*- and *meta*-xylene and TMB formation. Indeed, 1,2,3-TMB can only diffuse through straight channels and 1,3,5-TMB can only be formed on the external surface [45]. For ZSM-5 monolith 1,3,5-TMB is the major compound. The amount of TMB found is only 1.4 times less in comparison to commercial ZSM-5 and not 3 times as reasoned by the ratio of acid sites on external surface area. Hence, the higher *para*-xylene selectivity of ZSM-5 monolith might rather result from its unique morphology of particles composed of a 3D stacking of plate-like crystallites. It was indeed reported that for a similar toluene conversion of 3 % as for crushed ZSM-5 monolith, a very high *para*-xylene selectivity (99 %) was reached with ZSM-5 featuring plate-like intergrowth at the top of large ZSM-5 crystals (10 × 20 μm), leading to 73 % of pore openings through sinusoidal channel [6]. Plate-like crystals of ZSM-5 crystals present on their sides ([100] and [101] facets) the openings of sinusoidal channels and on the flat surface ([010] facet) the openings of straight channels [65]. It was shown previously that the intrinsic shape-selective ability enhances when ZSM-5 crystals stack on (010) plane forming one-dimensional *b*-oriented MFI superstructures [45]. It is to recall that TPA⁺ exerts a crucial role in the synthesis and promotes *b*-oriented assemblies. The sinusoidal channels are smaller (0.51 × 0.55 nm) and more tortuous than straight channels (0.53 × 0.56 nm). Small molecules diffuse readily in sinusoidal channels, while large molecules with diameter similar to those of sinusoidal channels tend to diffuse rather through the straight channels [45]. Toluene and *para*-xylene diffuse freely in both channels. Since the length of *para*-xylene (0.99 nm) exceeds the maximum diameter of the intersecting channels (~0.8 nm), it is difficult to switch from straight channels to sinusoidal channels, and *para*-xylene diffuse 8 times faster in straight channels. *Ortho*- and *meta*-xylenes only diffuse through straight channels [45]. This was further proven by size exclusion chromatography, where *ortho*- and *meta*-xylene were barely entering in the ZSM-5 crystals featuring a majority of pore openings through sinusoidal channels, in opposite to *para*-xylene [6]. The kinetic diameter of *para*-xylene is precisely comparable to the diameter of the sinusoidal channels, while the kinetic diameters of *meta*- and *ortho*-xylenes are larger [45]. Therefore, sinusoidal channels are more efficient for xylene isomers shape/size sieving and are the main reasons for the generation of higher *para*-xylene selectivity for plate-like shaped crystals. In ZSM-5 monoliths, the stacking of thin plate-like crystallites will hence result in maximum of pore openings through sinusoidal channels at the external surface through the side of the thin plates (Fig. 5). It is hence

possible to hypothesize that once *meta*- and *ortho*-xylenes are formed in the channel intersections, the only way to diffuse out of the ZSM-5 plate-like crystallites is to isomerize into *para*-xylene.

The very high selectivity in *para*-xylene of 99 % found in literature [6], in comparison to the one obtained with the crushed ZSM-5 monolith (68 %) is due to the combination of maximum openings through sinusoidal channels with: (i) a ZSM-5 featuring a very low Si/Al ratio of 148 and inverse Al gradient, leading to a low amount of Al at the external surface avoiding secondary *para*-xylene isomerization, while ZSM-5 monolith has high Al content (Si/Al = 43) with no Al gradient and hence higher concentration of acid sites on the external surface, (ii) high temperature (470 °C), which decreases slightly the size of sinusoidal and straight channels leading to higher shape selectivity and (iii) large ZSM-5 crystals (10 × 20 μm) in comparison to 3–6 μm particle size for ZSM-5 monolith(A) [6]. Larger ZSM-5 crystals are advantageous as increasing the crystal size of ZSM-5 above 10 μm should favor the isomerization of *meta*- and *ortho*-xylene by lengthen their pathway in the ZSM-5 channels and hence increase the *para*-xylene selectivity [61,62].

The ZSM-5 monolith was further tested as a single body catalytic microreactor (Fig. 8). For this purpose, the monolith was inserted in a borosilicate glass tube, as previously described by Jatou et al. [20] as an alternative to heat shrinkable PTFE clads [12,18,23,24,26,28]. This cladding approach features has the advantage to allow the in-flow use as microreactor even for temperature >250 °C.

Despite the low toluene conversion (1 %) a very high *para*-xylene selectivity of 81 % could be reached (Table 4). The increase in selectivity from 68 to 81 % between crushed monolith and the single catalytic body can most probably be ascribed to longer diffusion pathways in one-piece monolith (millimetric scale) in comparison to micronic particles of crushed monolith. The grinding could also cause the formation of some exposed plane facet with straight channel openings, allowing for increasing the out-diffusion of *meta*- and *ortho*-xylene from the crystallites.

The low value of toluene conversion obtained with H⁺-ZSM-5 monolith (Si/Al = 43) is certainly related to the chosen reaction conditions in order to avoid thermodynamic equilibrium of the *para*-/*meta*-/*ortho*-xylenes (24: 52: 24 %). However, as *para*-xylene selectivity with H⁺-ZSM-5 monolith is high (81 %), further optimizations of the catalytic conditions (higher temperature, higher toluene/MeOH ratio, longer contact time, higher H⁺ concentration, addition of H₂O, H₂, ...) might be envisaged. As ZSM-5 monoliths are stable at 470 °C in the presence of water harder conditions could be undertaken. It could be interesting to reproduce the conditions used by Wang et al. [6] for a ZSM-5 presenting maximum openings through sinusoidal channels, who co-fed H₂O and H₂ at temperature of 470 °C, with high amount of acid sites in the reactor reaching outstanding toluene conversion up to 50 % with 50 % MeOH efficiency and very high *para*-xylene selectivity of 99 %, although their ZSM-5 featured very low Si/Al ratio (148).

4. Conclusions

Pure H⁺-ZSM-5 monoliths (Si/Al ~ 40) with homogeneous network of macropores of 30–40 μm were obtained by a pseudomorphic transformation by steam assisted conversion of optimized aluminosilica monoliths prepared by a combination of sol-gel process and spinodal decomposition. The H⁺-ZSM-5 monoliths present a homogeneous



Fig. 8. H⁺-ZSM-5 monolith(A) inserted in a glass tube for the alkylation of toluene by methanol at 350 °C.

skeleton composed of a 3D aggregation of large particles of either 6 or 12 μm made of a 3D stacking of plate-like shape crystallites allowing for maximizing the openings of the external surface through sinusoidal channels. The H^+ -ZSM-5 monoliths were tested in the alkylation of toluene by methanol at 350 $^\circ\text{C}$ in packed-bed reactors with crushed powder and as catalytic microreactor through glass cladding. The particular shape of ZSM-5 particles in the skeleton and the low external surface area allowed for achieving a remarkably high *para*-xylene selectivity (81 %) in comparison to conventional commercial ZSM-5 (Si/Al = 40) (round/cubic crystallites morphology) presenting a *para*-xylene selectivity of 53 %. The conditions of the catalytic test remain to be optimized in order to reach high toluene conversion when using ZSM-5 monoliths as catalytic microreactors.

CRedit authorship contribution statement

Lucie Desmurs: Writing – review & editing, Methodology, Investigation, Conceptualization. **Claudia Cammarano:** Validation, Supervision, Formal analysis, Conceptualization. **Alexander Sachse:** Writing – review & editing, Formal analysis. **Olinda Gimello:** Formal analysis. **Thomas Gaillard:** Investigation. **Sacha Barberat:** Investigation. **Sebastien Blanquer:** Investigation. **Vasile Hulea:** Validation, Supervision. **Anne Galarneau:** Writing – review & editing, Writing – original draft, Validation, Supervision, Methodology, Investigation, Conceptualization.

Declaration of competing interest

The authors declare that they have no known competing financial interests or personal relationships that could have appeared to influence the work reported in this paper.

Data availability

Data will be made available on request.

Acknowledgments

The authors wish to acknowledge the support from the Chemistry Platform of Campus in Montpellier (Platform MEA University Montpellier), on which SEM and EDS have been performed, and especially Thomas Cacciaguerra and Didier Cot who took the SEM pictures of the monoliths. AS acknowledge the European Union (ERDF) and Région Nouvelle Aquitaine and the French government program “Investissements d’Avenir” (EUR INTREE, reference ANR-18-EURE-0010).

References

- W. Vermeiren, J.P. Gilson, Impact of zeolites on the petroleum and petrochemical industry, *Top. Catal.* 52 (2009) 1131–1161, <https://doi.org/10.1007/s11244-009-9271-8>.
- C. Martinez, A. Corma, Inorganic molecular sieves: preparation, modification and industrial application in catalytic processes, *Coord. Chem. Rev.* 255 (2011) 1558–1580, <https://doi.org/10.1016/j.ccr.2011.03.014>.
- Y. Li, J. Yu, Emerging applications of zeolites in catalysis, separation and host–guest assembly, *Nat. Rev. Mater.* 6 (2021) 1156–1174, <https://doi.org/10.1038/s41578-021-00347-3>.
- K. Tanabe, W. Holderich, Industrial application of solid acid-base catalysts, *Appl. Catal., A* 181 (1999) 399–434, [https://doi.org/10.1016/S0926-860X\(98\)00397-4](https://doi.org/10.1016/S0926-860X(98)00397-4).
- X. Huang, R. Wang, X. Pan, C. Wang, M. Fan, Y. Zhu, Y. Wang, J. Peng, Catalyst design strategies towards highly shape-selective HZSM-5 for *para*-xylene through toluene alkylation, *Green Energy Environ.* 5 (2020) 385–393, <https://doi.org/10.1016/j.gee.2019.12.00>.
- C. Wang, L. Zhang, X. Huang, Y. Zhu, G. Li, Q. Gu, J. Chen, L. Ma, X. Li, Q. He, J. Xu, Q. Sun, C. Song, M. Peng, J. Sun, D. Ma, Maximizing sinusoidal channels of HZSM-5 for high shape-selectivity to *p*-xylene, *Nat. Commun.* 10 (2019) 4348–4356, <https://doi.org/10.1038/s41467-019-12285-4>.
- J.S.J. Hargreaves, A.L. Munnoch, A survey of the influence of binders in zeolite catalysis, *Catal. Sci. Technol.* 3 (2013) 1165–1171, <https://doi.org/10.1039/C3CY20866D>.
- N.-L. Michels, S. Mitchell, J. Perez-Ramirez, Effects of binders on the performance of shaped hierarchical MFI zeolites in methanol-to-hydrocarbons, *ACS Catal.* 4 (2014) 2409–2417, <https://doi.org/10.1021/cs500353b>.
- K. Yang, D. Zhang, M. Zou, L. Yu, S. Huang, The known and overlooked sides of zeolite-extrudate catalysts, *ChemCatChem* 13 (2021) 1414–1423, <https://doi.org/10.1002/cctc.202001601>.
- A. Sachse, A. Galarneau, B. Coq, F. Fajula, Monolithic flow microreactors improve fine chemicals synthesis, *New J. Chem.* 35 (2011) 259–264, <https://doi.org/10.1039/C0NJ00965B>.
- A. Galarneau, Z. Abid, B. Said, Y. Didi, K. Szymanska, A. Jarzebski, F. Tancret, H. Hamaizi, A. Bengueddach, F. Di Renzo, F. Fajula, Synthesis and textural characterization of mesoporous and meso-/macroporous silica monoliths obtained by spinodal decomposition, *INORGA* 4 (2016) 9, <https://doi.org/10.3390/inorganics4020009>.
- A. El Kadib, R. Chimenton, A. Sachse, F. Fajula, A. Galarneau, B. Coq, Functionalized inorganic monolithic microreactors for high productivity in fine chemicals catalytic synthesis, *Angew. Chem. Int. Ed.* 48 (2009) 1–5, <https://doi.org/10.1002/anie.200805580>.
- X. Lu, K. Nakanishi, Synthesis of hierarchically porous metal oxide monoliths via sol–gel process accompanied by phase separation from divalent metal salts: a short review, *Front. Chem. Eng.* 3 (2021) 787788, <https://doi.org/10.3389/fceng.2021.787788>.
- A. Feinle, M.S. Elsaesser, N. Husing, Sol–gel synthesis of monolithic materials with hierarchical porosity, *Chem. Soc. Rev.* 45 (2016) 3377–3399, <https://doi.org/10.1039/c5cs00710k>.
- X. Lu, G. Hasegawa, K. Kanamori, K. Nakanishi, Hierarchically porous monoliths prepared via sol–gel process accompanied by spinodal decomposition, *J. Sol. Gel Sci. Technol.* 95 (2020) 530–550, <https://doi.org/10.1007/s10971-020-05370-4>.
- O.Y. Vodorezova, I.N. Lapin, T.I. Izaak, Formation of the open-cell foam structures in tetraethoxysilane-based gelling systems, *J. Sol. Gel Sci. Technol.* 94 (2020) 384–392, <https://doi.org/10.1007/s10971-020-05244-9>.
- A. Sachse, N. Linares, P. Barbaro, F. Fajula, A. Galarneau, Selective hydrogenation over Pd nanoparticles supported on a pore-flow-through silica monolith microreactor with hierarchical porosity, *Dalton Trans.* 42 (2013) 1378–1384, <https://doi.org/10.1039/c2dt31690k>.
- A. Galarneau, A. Sachse, B. Said, C.-H. Pelisson, P. Boscaro, N. Brun, L. Courtheoux, N. Olivi-Tran, B. Coasne, F. Fajula, Hierarchical porous silica monoliths: a novel class of microreactors for process intensification in catalysis and adsorption, *C. R. Chimie* 19 (2016) 231–247, <https://doi.org/10.1016/j.crci.2015.05.017>.
- D. Enke, R. Glaser, U. Tallarek, Sol-gel and porous glass-based silica monoliths with hierarchical pore structure for solid-liquid catalysis, *Chem. Ing. Tech.* 88 (2016) 1–26, <https://doi.org/10.1002/cite.201600049>.
- H.U.K. Jatoti, M. Goepel, D. Poppitz, R. Kohns, D. Enke, M. Hartmann, R. Glaser, Mass Transfer in hierarchical silica monoliths loaded with Pt in the continuous-flow liquid-phase hydrogenation of *p*-nitrophenol, *Front. Chem. Eng.* 3 (2021) 789416, <https://doi.org/10.3389/fceng.2021.789416>.
- K. Szymanska, A. Ciemiega, K. Maresz, W. Pudlo, J. Malinowski, J. Mrowiec-Bialon, A.B. Jarzebski, Catalytic functionalized structured monolithic micro-/mesoreactors: engineering, properties, and performance in flow synthesis: an overview and guidelines, *Front. Chem. Eng.* 3 (2021) 789102, <https://doi.org/10.3389/fceng.2021.789102>.
- M. Marelli, F. Zaccheria, N. Ravasio, E. Pitzalis, Y. Didi, A. Galarneau, N. Scotti, C. Evangelisti, Copper oxide Nanoparticles over hierarchical silica monoliths for continuous-flow selective alcoholysis of styrene oxide, *Catalysts* 13 (2023) 341, <https://doi.org/10.3390/catal13020341>.
- A. Sachse, A. Galarneau, F. Di Renzo, F. Fajula, B. Coq, Synthesis of zeolite monoliths for flow continuous processes. The case of sodalite as a basic catalyst, *Chem. Mater.* 22 (2010) 4123–4125, <https://doi.org/10.1021/cm1014064>.
- A. Sachse, A. Galarneau, F. Di Renzo, P. Creux, F. Fajula, B. Coq, Functional silicic monoliths with hierarchical uniform porosity as continuous flow catalytic reactors, *Microporous Mesoporous Mater.* 140 (2011) 58–68, <https://doi.org/10.1016/j.micromeso.2010.10.044>.
- B. Said, T. Cacciaguerra, F. Tancret, F. Fajula, A. Galarneau, Size control of self-supported LTA zeolite nanoparticles monoliths, *Microporous Mesoporous Mater.* 227 (2016) 176–190, <https://doi.org/10.1016/j.micromeso.2016.02.048>.
- B. Said, A. Grandjean, Y. Barre, F. Tancret, F. Fajula, A. Galarneau, LTA zeolite monoliths with hierarchical trimodal porosity as highly efficient microreactors for strontium capture in continuous flow, *Microporous Mesoporous Mater.* 232 (2016) 39–52, <https://doi.org/10.1016/j.micromeso.2016.05.036>.
- Y. Didi, B. Said, T. Cacciaguerra, K.L. Nguyen, V. Wernert, R. Denoyel, D. Cot, W. Sebai, M.-P. Belleville, J. Sanchez-Marcano, F. Fajula, A. Galarneau, Synthesis of binderless FAU-X (13X) monoliths with hierarchical porosity, *Microporous Mesoporous Mater.* 281 (2019) 57–65, <https://doi.org/10.1016/j.micromeso.2019.03.003>.
- Y. Didi, B. Said, M. Micolle, T. Cacciaguerra, D. Cot, A. Geneste, F. Fajula, A. Galarneau, Nanocrystals FAU-X monoliths as highly efficient microreactors for cesium capture in continuous flow, *Microporous Mesoporous Mater.* 285 (2019) 185–194, <https://doi.org/10.1016/j.micromeso.2019.05.012>.
- Q. Lei, T. Zhao, F. Li, Y. Wang, N. Sun, Zeolite beta monoliths with hierarchical porosity by the transformation of bimodal pore silica gel, *J. Porous Mater.* 15 (2008) 643–646, <https://doi.org/10.1007/s10934-007-9144-0>.
- Q. Lei, T. Zhao, F. Li, L. Zhang, Y. Wang, Catalytic cracking of large molecules over hierarchical zeolites, *Chem. Commun.* (2006) 1769–1771, <https://doi.org/10.1039/b600547k>.

- [31] Q. Lei, T. Zhao, F. Li, Y. Wang, M. Zheng, Fabrication of hierarchically structured monolithic silicalite-1 through steam-assisted conversion of macroporous silica gel, *Chem. Lett.* 35 (2006) 490–491, <https://doi.org/10.1246/cl.2006.490>.
- [32] T. Zhao, X. Xu, Y. Tong, Q. Lei, F. Li, L. Zhang, The synthesis of novel hierarchical zeolites and their performances in cracking large molecules, *Catal. Lett.* 136 (2010) 266–270, <https://doi.org/10.1007/s10562-009-0131-8>.
- [33] W.-C. Li, A.-H. Lu, R. Palkovits, W. Schmidt, B. Spliethoff, F. Schüth, Hierarchically structured monolithic silicalite-1 consisting of crystallized nanoparticles and its performance in the Beckmann rearrangement of cyclohexanone oxime, *J. Am. Chem. Soc.* 127 (2005) 12595–12600, <https://doi.org/10.1021/ja052693>.
- [34] Y. Tong, T. Zhao, F. Li, Y. Wang, Synthesis of monolithic zeolite beta with hierarchical porosity using carbon as a transitional template, *Chem. Mater.* 18 (2006) 4218–4220, <https://doi.org/10.1021/cm060035j>.
- [35] T. Zhao, W. Jia, X. Xin, W. Guijie, Preparation of hierarchically trimodal-porous ZSM-5 composites through steam-assisted conversion of macroporous aluminosilica gel with two different quaternary ammonium hydroxides, *China Petrol. Proc. & Petrochem. Techn.* 17 (2015) 48–58.
- [36] K. Moukahlal, N.H. Le, M. Bonne, J. Toufaily, T. Hamieh, T.J. Daou, B. Lebeau, Controlled crystallization of hierarchical monoliths composed of nanozeolites, *Cryst. Growth Des.* 20 (2020) 5413–5423, <https://doi.org/10.1021/acs.cgd.0c00631>.
- [37] H. Yang, Q. Liu, Z. Liu, H. Gai, Z. Xie, Controllable synthesis of aluminosilica monoliths with hierarchical pore structure and their catalytic performance, *Microporous Mesoporous Mater.* 127 (2010) 213–218, <https://doi.org/10.1016/j.micromeso.2009.07.016>.
- [38] A.C. Marques, M. Vale, Macroporosity control by phase separation in sol-gel derived monoliths and microspheres, *Materials* 14 (2021) 4247, <https://doi.org/10.3390/ma14154247>.
- [39] S. Murai, K. Fujita, K. Nakanishi, K. Hirao, Morphology control of phase-separation-induced alumina-silica macroporous gels for rare-earth-doped scattering media, *J. Phys. Chem. B* 108 (2004) 16670–16676, <https://doi.org/10.1021/jp0481658>.
- [40] J. Wu, X. Li, W. Du, C. Dong, L. Li, Preparation and characterization of bimodal porous alumina-silica and its application to removal of basic nitrogen compounds from light oil, *J. Mater. Chem.* 17 (2007) 2233–2240.
- [41] R. Takahashi, S. Sato, T. Sodesawa, M. Yabuki, Silica-alumina catalyst with bimodal pore structure prepared by phase separation in sol-gel process, *J. Catal.* 200 (2001) 197–202, <https://doi.org/10.1006/jcat.2001.319>.
- [42] W. Sebai, S. Ahmad, M.-P. Belleville, A. Boccheciampe, P. Chaurand, C. Levard, N. Brun, A. Galarneau, J. Sanchez-Marcano, Biocatalytic elimination of pharmaceuticals found in water with hierarchical silica monoliths in continuous flow, *Front. Chem. Eng.* 4 (2022) 823877, <https://doi.org/10.3389/fceng.2022.823877>.
- [43] L. Desmurs, A. Galarneau, C. Cammarano, V. Hulea, C. Vaulot, H. Nouali, B. Lebeau, T.J. Daou, C. Vieira Soares, G. Maurin, M. Haranczyk, I. Batonneau-Gener, A. Sachse, Determination of microporous and mesoporous surface areas and volumes of mesoporous zeolites by corrected t-plot analysis, *Chem. Nano. Mat.* 8 (2022) e202200051, <https://doi.org/10.1002/cnma.202200051>.
- [44] T. Martin, A. Galarneau, F. Di Renzo, F. Fajula, D. Plee, Morphological control of mcm-41 by pseudomorphic synthesis, *Angew. Chem. Int. Ed.* 41 (2002) 2590–2592, [https://doi.org/10.1002/1521-3773\(20020715\)41:14<2590::AID-ANIE2590>3.0.CO;2-3](https://doi.org/10.1002/1521-3773(20020715)41:14<2590::AID-ANIE2590>3.0.CO;2-3).
- [45] L. Zhang, N. Liu, C. Dai, R. Xu, G. Yu, B. Chen, N. Wang, Recent advances in shape selectivity of MFI zeolite and its effect on the catalytic performance, *Chem. Synth.* 3 (2022) 2, <https://doi.org/10.20517/cs.2022.31>.
- [46] X. Mi, Z. Hou, X. Li, Controllable synthesis of nanoscaled ZSM-5 aggregates with multivariate channel under the synergistic effect of silicate-1 and TPABr using dual-silica source, *Microporous Mesoporous Mater.* 323 (2021) 111224, <https://doi.org/10.1016/j.micromeso.2021.111224>.
- [47] T. Yokoi, H. Mochizuki, S. Namba, J.N. Kondo, T. Tatsumi, Control of the Al distribution in the framework of ZSM-5 zeolite and its evaluation by solid-state NMR technique and catalytic properties, *J. Phys. Chem. C* 119 (2015) 15303–15315, <https://doi.org/10.1021/acs.jpcc.5b03289>.
- [48] S. Ezenwa, H. Montalvo-Castra, A.J. Hoffman, H. Locht, J. Attebery, D.-Y. Jan, M. Schmithorst, B. Chmelka, D. Hibbits, R. Gounder, Synthetic placement of active sites in MFI zeolites for selective toluene methylation to para-xylene, *J. Am. Chem. Soc.* (2024), <https://doi.org/10.1021/jacs.4c00373>.
- [49] E. Dib, J. Grand, A. Gedeon, S. Mintova, C. Fernandez, Control the position of framework defects in zeolites by changing the symmetry of organic structure directing agents, *Microporous Mesoporous Mater.* 315 (2021) 110899, <https://doi.org/10.1016/j.micromeso.2021.110899>.
- [50] A. Zecchina, L. Marchese, S. Bordiga, C. Paze, E. Gianotti, Vibrational spectroscopy of NH₄⁺ ions in zeolitic materials: an IR study, *J. Phys. Chem. B* 101 (1997) 10128–10135, <https://doi.org/10.1021/jp9717554>.
- [51] B. Hunger, M. Heuchel, L.A. Clark, R.Q. Snurr, Characterization of acidic OH groups in zeolites of different types: an interpretation of NH₃-TPD results in the light of confinement effects, *J. Phys. Chem. B* 106 (2002) 3882–3889, <https://doi.org/10.1021/jp012688n>.
- [52] C.L. Padro, C.R. Apesteguia, Acylation of phenol on solid acids: study of the deactivation mechanism, *Catal. Today* 107–108 (2005) 258–265, <https://doi.org/10.1016/j.cattod.2005.07.078>.
- [53] M. Takeuchi, T. Tsukamoto, A. Kondo, M. Masuoka, Investigation of NH₃ and NH₄⁺ adsorbed on ZSM-5 zeolites by near and middle infrared spectroscopy, *Catal. Sci. Technol.* 5 (2015) 4587–4593, <https://doi.org/10.1039/c5cy00753d>.
- [54] L. Desmurs, C. Cammarano, G. Ramona, R. Gaumard, T. Mineva, A. Sachse, J.-D. Comparot, T. Cacciaguerra, D. Cot, O. Gimello, A. Galarneau, V. Hulea, Finding the compromise between Bronsted acidity and mesoporosity in hierarchical micro-/mesoporous ZSM-5? *ChemCatChem* 15 (2023) e202300167 <https://doi.org/10.1002/cctc.202300167>.
- [55] E.K.H. Salje, J. Koppensteiner, W. Schranz, E. Fritsch, Elastic instabilities in dry, mesoporous minerals and their relevance to geological, *Appl. Mineral Mag.* 74 (2010) 341–350, <https://doi.org/10.1180/minmag.2010.074.2.341>.
- [56] J. Cejka, B. Wichterlová, G. Eder-Mirth, J.A. Lercher, Decisive role of transport rate of products for zeolite para-selectivity: effect of coke deposition and external surface silylation on activity and selectivity of HZSM-5 in alkylation of toluene, *Zeolites* 17 (1996) 265–271, [https://doi.org/10.1016/0144-2449\(96\)00006-1](https://doi.org/10.1016/0144-2449(96)00006-1).
- [57] W. Tan, M. Liu, Y. Zhao, K. Hou, H. Wu, A. Zhang, H. Liu, Y. Wang, C. Song, X. Guo, Para-selective methylation of toluene with methanol over nano-sized ZSM-5 catalysts: synergistic effects of surface modifications with SiO₂, P2O₅ and MgO, *Microporous Mesoporous Mater.* 196 (196) (2014) 18–30, <https://doi.org/10.1016/j.micromeso.2014.04.050>.
- [58] S. Zheng, H.R. Heydenrych, A. Jentys, J.A. Lercher, Influence of surface modification on the acid site distribution of HZSM-5, *J. Phys. Chem. B* 106 (2002) 9552–9558, <https://doi.org/10.1021/jp014091d>.
- [59] C. Wang, Q. Zhang, Y. Zhu, D. Zhang, J. Chen, F.-K. Chiang, p-Xylene selectivity enhancement in methanol toluene alkylation by separation of catalysis function and shape-selective function, *Mol. Catal.* 433 (2017) 242–249, <https://doi.org/10.1016/j.mcat.2016.12.007>.
- [60] Y.S. Bhat, J. Das, K.V. Rao, A.B. Halgeri, Inactivation of external surface of ZSM-5: zeolite morphology, crystal size, and catalytic activity, *J. Catal.* 159 (1996) 368–374, <https://doi.org/10.1006/jcat.1996.0099>.
- [61] L.B. Young, S.A. Butter, W.W. Kaeding, Shape selective reactions with zeolite catalysts: III. Selectivity in xylene isomerization, toluene-methanol alkylation, and toluene disproportionation over ZSM-5 zeolite catalysts, *J. Catal.* 76 (1982) 418–432, [https://doi.org/10.1016/0021-9517\(82\)90271-8](https://doi.org/10.1016/0021-9517(82)90271-8).
- [62] J. Breen, R. Burch, M. Kulkarni, P. Collier, S.J. Golunski, Enhanced para-xylene selectivity in the toluene alkylation reaction at ultralow contact time, *J. Am. Chem. Soc.* 127 (2005) 5020–5021, <https://doi.org/10.1021/ja046421o>.
- [63] W. Alabi, L. Atanda, R. Jermy, S. Al-Khattaf, Kinetics of toluene alkylation with methanol catalyzed by pure and hybridized HZSM-5 catalysts, *Chem. Eng. J.* 195–165 (2012) 276–288, <https://doi.org/10.1016/j.cej.2012.04.100>.
- [64] L. Desmurs, C. Cammarano, O. Gimello, A. Galarneau, V. Hulea, Influence of the mesoporosity of hierarchical ZSM-5 in the toluene alkylation by methanol, *Materials* 16 (2023) 6872, <https://doi.org/10.3390/ma16216872>.
- [65] X. Liu, J. Shi, G. Yang, J. Zhou, C. Wang, J. Teng, Y. Wang, Z. Xie, A diffusion anisotropy descriptor links morphology effects of H-ZSM-5 zeolites to their catalytic cracking performance, *Commun. Chem.* 4 (2021) 107, <https://doi.org/10.1038/s42004-021-00543-w>.